High Ratio Non-Isolated DC–DC Converter for Hydrogen Battery Using a 50 kW PEM Fuel Cell

Nicolas Videau, Guillaume Fontès, Didier Flumian, Guillaume Gateau, Thierry A. Meynard, João Lucas Da Silva, O. Verdu

High Ratio Non-Isolated DC–DC Converter for Hydrogen Battery Using a 50kW PEM Fuel Cell*

N. Videau[1*], G. Fontes[1], D. Flumian[1], G. Gateau[1], T. Meynard[1], J.L. da Silva[1], O. Verdu[2]

[1] **Laboratoire LAPLACE, Université de Toulouse, 2 rue Charles Camichel, Toulouse, France**
[2]**Areva Stockage d'Energie, Avenue Louis Philibert, Aix-en-Provence, France**

Abstract

This paper proposes a DC–DC converter dedicated to high efficiency and high voltage conversion ratio, which is well suited for fuel cell applications. At high voltage conversion ratio the proposed converter, named here mirror boost converter, has a better ratio of active/freewheeling times which, compared with conventional structures, reduces the penalty on efficiency induced by the high conversion ratio. This converter also uses eight interleaved coupled-inductors, which reduces the current and voltage ripple and makes possible to use of smaller passive components. Coupling all phases with an inter-cell transformer (ICT) also improves the power density, volume and losses of the magnetic component compared to separate inductors. A comparison with a classical double boost converter is realized using the same material. The proposed converter reaches a peak efficiency of 96.5% at 17 kW and 95.3% at 42 kW for a voltage conversion ratio around 10. The mirror boost converter has about half the losses of the double boost converter at same fuel cell power and delivers 69% more power at the maximum measured current phase.

Keywords: Ageing, DC–DC Power Converter, Energy Conversion, Fuel Cell, High Efficiency Converter, High Voltage Ratio Converter, Hydrogen Storage, Hydrogen Battery, Inter-Cell Transformer, Mirror Converter

1 Introduction

The development of renewable energy seems inevitable in order to face the current and future energy demands. However, electricity production from wind or solar sources is intermittent and unpredictable. For this reason, storage systems are required to smooth production and supply energy when demand exceeds production.

Among the different available technologies, the hydrogen battery – composed of two electrochemical components (electrolyzer and fuel cell) and gas storage tanks for the hydrogen H_2 and the oxygen O_2 (Figure 1) – seems to be a promising solution due to the following reasons [1]:

(i) Coupled with renewable energy sources, hydrogen battery produces carbon-free electricity, i.e. without any greenhouse gas emission.
(ii) The stored energy and power of the system are decoupled: basically, the stored energy is related to the size of the gas tank while the system power depends on the characteristics of the electrochemical components and on the design of the power electronics converter (PEC) connecting these latter to the grid.
(iii) Unlike their counterpart storage solutions as PSH (pumped-stored hydroelectricity) and CAES (compressed air energy storage), hydrogen batteries can be built in modular system which are easily transportable and usable everywhere.

During electricity overproduction periods, the hydrogen and oxygen gases produced by the electrolyzer are stored [2].

[*] *Paper presented at the 6th International Conference on Fundamentals and Development of Fuel Cells (FDFC2015), February 3 – 5, 2015 held in Toulouse, France.*

[*] *Corresponding author, nicolas.videau@laplace.univ-tlse.fr*

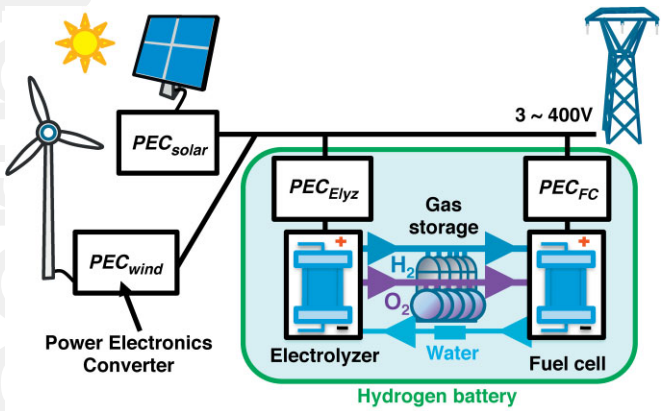

Fig. 1 Hydrogen battery coupled with renewable sources.

During high electricity demand periods or to smooth the renewable source production, the fuel cell converts the stored hydrogen into electricity. As long as the fuel cell is supplied with gas, the hydrogen battery produces electricity typically for one hour up to several days. The output power ranges from a few kilowatts (kW) to several megawatts (MW) (hydrogen farms containing several systems in parallel).

Typical power electronics converters (PEC) connecting the electrochemical component to the grid use a low voltage inverter and a low frequency (LF) transformer (50 Hz or 60 Hz). It provides a galvanic isolation and increases the voltage (Figure 2a) to reach the three-phase grid voltage (typically 400 Vrms) since electrochemical components have low-voltage high-current characteristics. As discussed in [1], this last solution has thus several benefits but produces continuously copper and core losses [3]. A few other power conversion solutions use an isolated DC–DC converter (including a high frequency transformer which helps to increase the voltage) and a medium voltage inverter, but the transformer shows also high losses. As cost is a key parameter, achieving high efficiency reduces the operating cost and increases the system autonomy, and higher efficiencies are achievable with transformer-less topologies [4]. Indeed, transformer-less power converters have received a research effort for a long time: in photovoltaic systems for example, as underlined in [5]. In fuel cell systems, transformer-less solutions (Figure 2b) could also be interesting but must be carefully evaluated because the required voltage step-up ratio is high and efficiencies of DC–DC converters with high voltage step-up ratio are often low. In the end the improvement of efficiency is not guaranteed at all.

The proposed study will focus on the DC–DC converter elevating the output fuel cell voltage to a 700 V DC bus required for the inverter connected to the three-phase grid. With a nominal 50 kW fuel cell voltage in a range of 60–70 V, the DC–DC converter operates with a voltage ratio higher than 10. In this condition, the traditional boost converter rapidly shows its limitation due to parasitic elements and the use of a constrained duty cycle D [1, 6]. The double boost converter [1, 6, 7] appears as a more relevant choice mainly because of its multilevel structure allowing the converter to use power devices with a lower voltage rating, i.e. more efficient semi-conductors. Sharing the same transfer function as the boost converter, the double boost converter requires a high duty cycle limiting its performance at high voltage ratio. Cascaded boost converter is not also an option because of the low efficiency of the overall conversion. In 2006, O. Rallières [6] introduces what we named in this paper a mirror boost converter with two phases and highlights its capability to manage high voltage ratio thanks to a non-standard arrangement of the two commutation cells. Since then, few papers have presented results with two or more phases with independent inductors for step-up conversion [9–11]. In [12], the feasibility of using an inter-cell transformer (ICT) instead of uncoupled inductors in a mirror boost converter has been presented, which makes possible to get a low current ripple (usually required for fuel cells and electrolyzers) with a smaller volume of magnetic elements.

The main objectives of this paper are presenting the mirror boost converter with eight interleaved phases, all of them being magnetically coupled with an ICT, showing its suitability for a fuel cell operation during its lifetime and comparing experimental results with the proposed converter and a double boost using the same material.

The first part of this paper presents the electrical features of the fuel cell used as hypothesis for the experiments. In the second part, the main features of the mirror boost converter are introduced. The final part is dedicated to experimental results and to the comparison between the double boost and the mirror boost converter using the same modular reconfigurable converter. Efficiency waveforms are derived from converter loss measurement obtained by the opposition method in order to ensure accurate measurements.

2 Requirements for the Power Converters

2.1 High Efficiency High Voltage Ratio DC–DC Converter

Proton exchange membrane technology is ideal for stationary application mainly because PEM fuel cell (FC) or electroly-

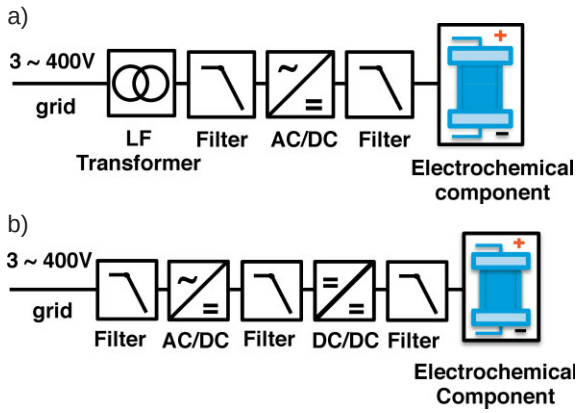

Fig. 2 Power electronics converter connecting the electrochemical com-ponent to the grid a) with a low frequency (LF) transformer, b) transform-less solution.

zer (Elyz) operates at low temperature (typ. 70–80 °C), low pressure (typ. FC: 1–5 bars, Elyz: 1–50 bars) and they have a high power density. Moreover, they offer a quick start-up time compared to high temperature fuel cells thanks to their cold start capability. Since elementary cells operate at low output voltage (typ. FC: $V_{cell,FC}$ = 0.6–0.7 V, Elyz: $V_{cell,Elyz}$ = 1.8–2 V with a current density around 1 to 2 A cm^{-2}), electrochemical components are realized by staking cells in series to increase the output voltage and cooling tubes are implemented in parallel. The assembly with graphite bipolar plates is limited to 100–150 cells in series, due to the increased complexity and cost adding to the decline reliability and lifetime of the system.

The considered electrochemical components in this paper are composed of 100 cells in series to reduce the drawbacks presented above leading to a fuel cell stack open circuit voltage around 100 V and a nominal voltage in the range 60 V to 70 V. In the case of the electrolyzer stack, the open circuit voltage is around 140 V with a nominal voltage in the range of 180 V to 200 V. Because of a fuel cell stack voltage lower than the electrolyzer stack voltage and thus more constraining, the DC–DC converter proposed in this paper is developed with the fuel cell voltage characteristic. It can be noted this converter has also been designed for the electrolyzer and is thus reversible. Efficiency results will be higher with the electrolyzer stack thanks to a lower voltage ratio required.

The static characteristics voltage-current and power-current of the PEM fuel cell considered in this paper are shown in Figure 3a. The fuel cell is composed of 100 elementary cells with an active area of 600 cm^2. The fuel cell operates at 60 °C and 2 bars. The values of the parameters used are shown in Table 1 and the static voltage curve $V_{FC}(I_{FC})$ follows equation 1 developed in [13]:

$$V_{FC} = n_{cells} V_{cell} = n_{cells}\left(E_{th} - \frac{RT}{\alpha nF} ln\left(\frac{I_{FC}}{I_0}\right) - R_{mem} I_{FC}\right) \quad (1)$$

where n_{cells} is the number of elementary cells in series, V_{cell} the voltage of an elementary cell and I_{FC} the fuel cell current. The others parameters definition are given in Table 1.

The fuel cell operations of the beginning of life (NEW) and end of life (EOL) are represented. At EOL, the characteristic voltage-current of the fuel cell is deteriorated mainly because of catalyst loss, membrane degradation and deterioration of the diffusion layers [14, 15]. For its application (a green power generator) the fuel cell manufacturer wanted that both beginning of life and end of life provide this same nominal power. This can only be performed by trading voltage for current during the fuel cell life. The fuel cell voltage at the beginning of life is equal to 70V@715A and decreases at EOL to 59V@849A. The

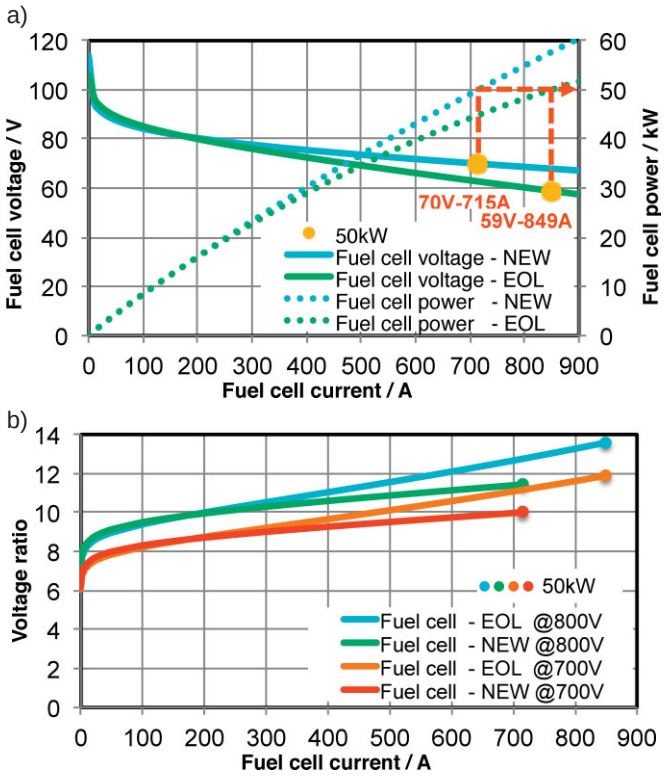

Fig. 3 a) Fuel cell voltage and fuel cell power versus current; b) Voltage ratio versus fuel cell current.

low-voltage high-current feature of the fuel cell appears clearly. With the fuel cell aging, this phenomenon is even more pronounced.

Figure 3b shows the voltage ratio of the DC–DC converter connecting the fuel cell to the DC bus. With a typical DC bus of 700 V required for the inverter connected to the 400 V 3-phase grid (800 V is typically used for the 480 V 3-phase), the voltage ratio is greater than 8. At nominal power, the voltage ratio is equal to 10 at the beginning of fuel cell life and reaches around 12 at the end of fuel cell life. Voltage ratio is even more elevated with a voltage DC bus of 800 V. Such high voltage ratios with a requirement for high efficiency lead to investigate non-conventional topologies as presented below.

Table 1 Fuel cell 50kW- parameters.

	Beginning of life (NEW)	End of life (EOL)
R Molar gas constant	8.314 J mol^{-1} K^{-1}	
F Faraday constant	96485 C mol^{-1}	
n Number of exchanged electrons per mole of reactant	2	
T Temperature	333 K	
E_{th} reversible voltage including effect of gas pressures	1.1 V	
α Global transfer coefficient	0.350	
I_0 Activation current	240 mA	420 mA
R_{mem} Resistance of the membrane	0.1 mΩ	0.233 mΩ

2.2 Fuel Cell Current Ripple Limitation

Requirements for fuel cell current ripples are still not clear. On one hand, G. Fontes et al. [13] has shown the fundamental role of electrochemical double layer phenomena, equivalent to an electric capacitor, which provides an internal filtering of high-frequency current ripple produced by DC/DC converters, but with no idea on the possible consequences on the membrane ageing or on the fuel consumption. On the other hand, D. Guilbert et al. [16] has made a brief review of the influences of high frequency current ripples (mostly often of 20%), and underlines that a huge disparity between the different results or consequences on the fuel cell degradation can be noticed. Yet, it seems that high frequency current ripples are not favorable for the fuel cell lifetime and should be reduced, and should be "far" below the 20% considered.

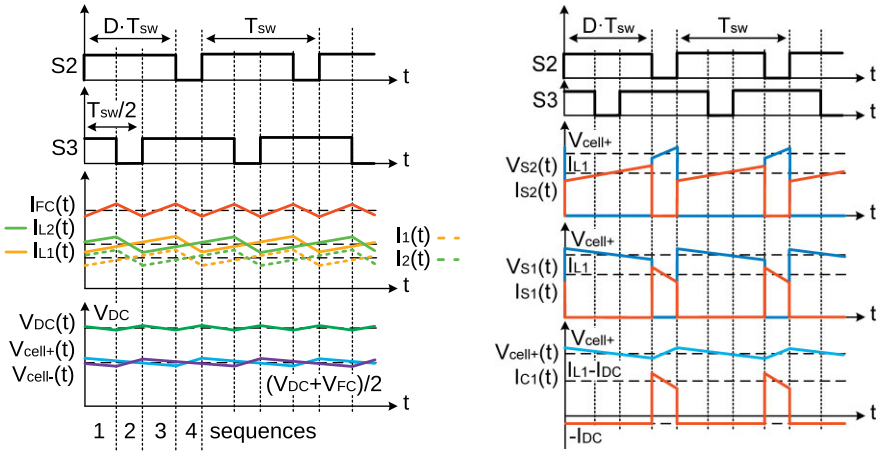

Fig. 5 Theoretical waveforms.

3 Proposed Mirror Boost Converter

The elementary topology of the proposed converter is of two floating boost converters in a non-standard configuration (Figure 4). The main waveforms of the converter are illustrated in Figure 5 and the operating sequences are presented in Figure 6. The mirror boost converter has both the benefits of series and parallel topologies. With the adequate control, if all the losses and imperfections (in inductors and semi-conductors) are neglected, the two floating voltages $V_{cell-/+}$ are equal to:

$$V_{Cell-/+} = \frac{V_{FC} + V_{DC}}{2} = \frac{V_{FC}}{(1-D)} = \frac{V_{DC}}{(1+D)} \tag{2}$$

with D the duty cycle of the semiconductors S_2 and S_3. At high voltage ratio, the semiconductor voltage constraints are reduced compare to the output converter voltage. This feature decreases the switching losses compare to a classical boost.

Figure 8 shows the parallel aspect of the topology. The most used power devices (S_2 and S_3) have substantially similar constraints than the interleaved 2 phases boost converter which is favorable for the efficiency. Moreover, the mirror boost con-

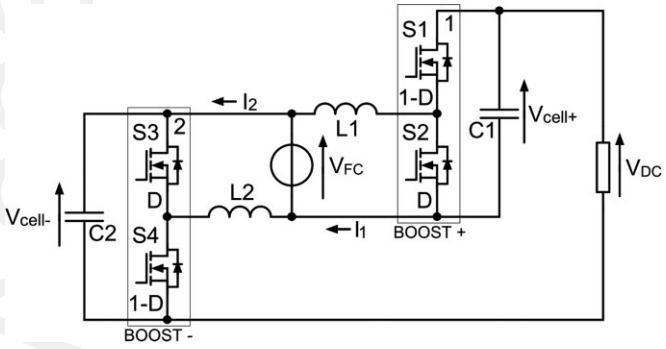

Fig. 4 Mirror boost.

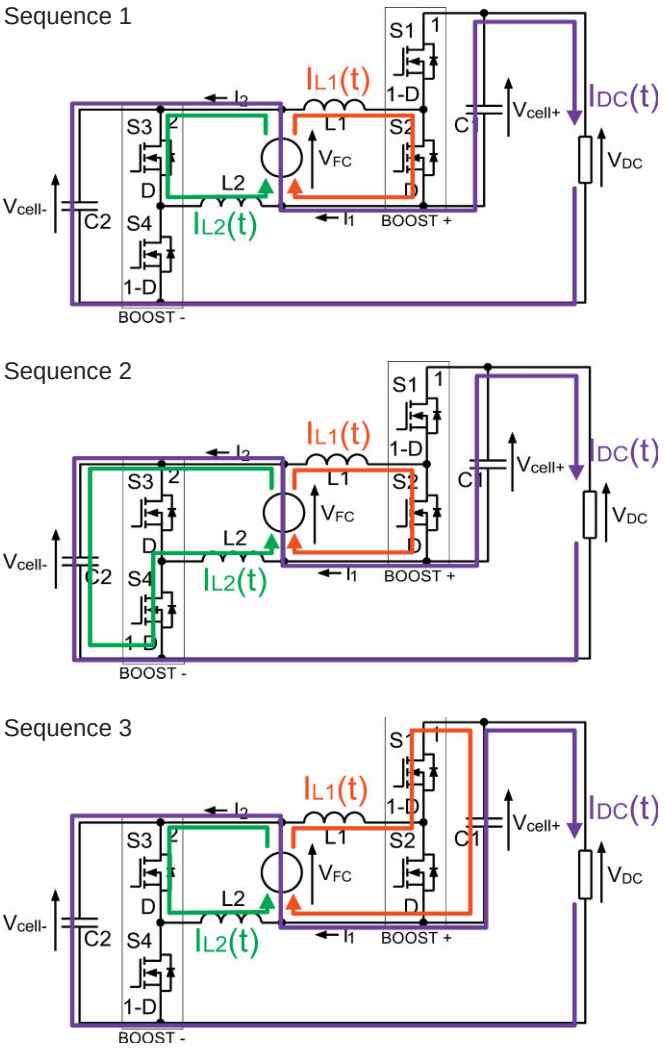

Fig. 6 Operating sequences.

verter has a better ratio of active/freewheeling times which, compared with conventional structures, reduces the penalty induced by the high conversion ratio given by (Figure 7a):

$$\frac{V_{DC}}{V_{FC}} = \frac{(1+D)}{(1-D)} \tag{3}$$

Voltage and current constraints and interleaved operation make possible the use of smaller passive components than conventional topologies. As shown in Figure 7b, the total energy of the inductive components of the mirror boost converter is lower than their counterpart classical converter (boost and double boost converter) leading to lower volume and weight inductive components (in this case of low current ripples and with same technology) [1]. The total energy of the capacitive components of the mirror boost converter is lower than conventional converter leading to smaller volume and weight capacitive components.

4 Experimental Results and Discussion

4.1 Prototype

The electrical schematic of the proposed converter is shown in Figure 9a. The fuel cell is emulated by a 45 kW ACORE power source which reproduces the voltage-current characteristic in Figure 3a. The load is made from a 0–150 kVA resistive bank. Figure 10 shows a picture of the experiment setup. The mirror boost is realized from a prototype power converter designed by Schneider Electric – APC initially devoted to an eight-phase double boost converter (Figure 11).

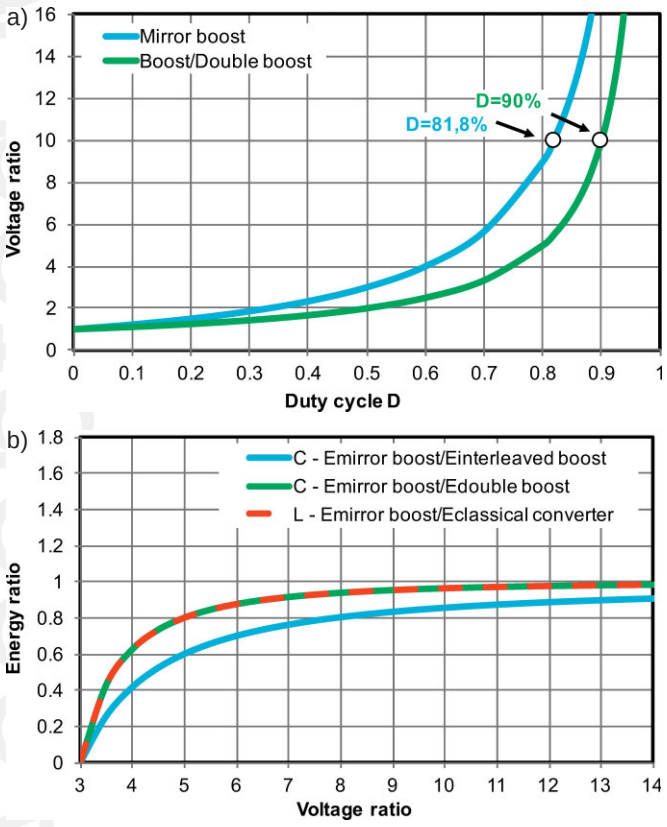

Fig. 7 Mirror boost converter a) duty cycle D, b) total energy in passive elements.

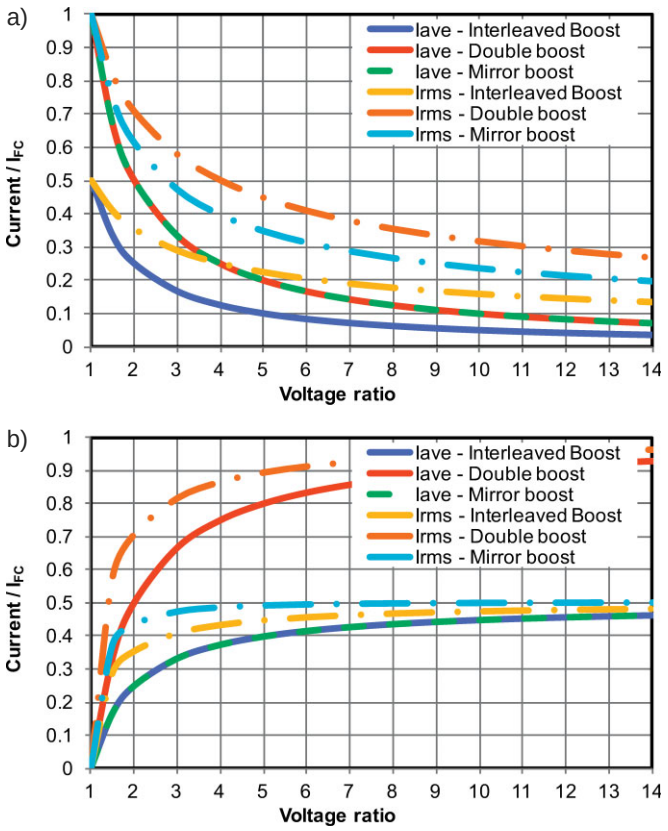

Fig. 8 Current semiconductors constraints a) 1-D (S1 & S4). b) D (S2 & S3).

The configuration of each commutation cell is illustrated in Figure 9b. The control switch is composed of direct paralleling of 3 IGBTs with their associated antiparallel diodes (IKW75N60H3, 600 V, 75 A) with a power metal-oxide-semiconductor field-effect transistor (MOSFET) (IPW65R041CFD, 650 V, 43 A). This combination makes possible to use the low conduction characteristic losses of the IGBT and the reduced turn-off losses of the MOSFET. The non-controlled switches consist of direct paralleling 3 SiC Schottky diodes modules (SCS140AE2, 600 V, 40 A). The ICT is designed to support a phase maximal current of 90 A and a 400 V voltage operating at a switching frequency f_{sw} of 20 kHz. Details of the ICT design are given in [7]. The switch PWM patterns are generated by an ALTERA DE2-115 board containing a field programmable gate array (FPGA: Cyclone IV EP4CE115). The eight-phase signals are phase shift of 45° (360°/8) and the phase order is determined to minimize the flux in the magnetic core [1]. The converter is controlled in close-loop in order to:

(i) regulate the DC bus voltage to 700 V;
(ii) balance the floating voltage $V_{cell+/-}$;

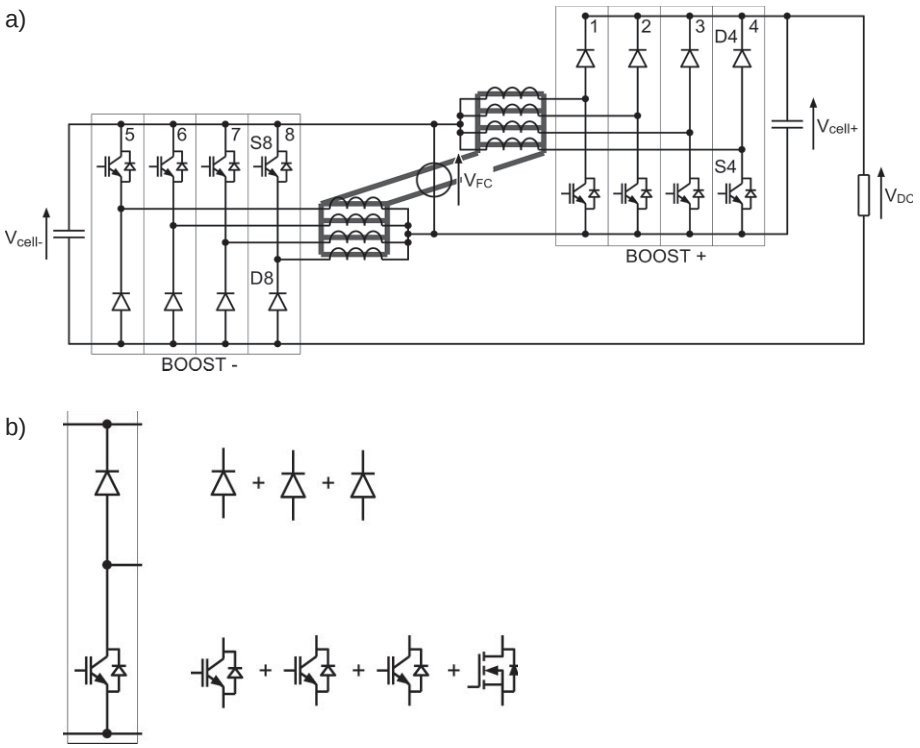

Fig. 9 a) Electrical schematic of the proposed mirror boost converter, b) Commutation cell.

(iii) balance phase currents and thus to avoid the saturation of the magnetic field leading to short-circuit (a maximum of 1 A of unbalance current is tolerate).

4.2 Experimental Results

Figure 12 shows the waveforms of the current source I_{FC}, the current in phase 2 I_2, the load current I_{DC} and the phase voltage V_{ph1} under a duty cycle D = 79.4% (voltage ratio of 8.7) and an output power of 11.2 kW. The power supply is composed of a three-phase rectifier leading to a significant component at 300 Hz ($6{\cdot}f_{grid}$) in the source current thus in the phases current. The effective switching frequency of the source is 160 kHz, which is 8 times the power device switching frequency. The observed current ripple is around 12% at this operating point and is less than 2.5% at the maximal converter operating point from simulation ($I_{ph,MAX}$ = 90 A , $P_{FC,NEW}$ = 46 kW). The parallel aspect of the mirror boost converter and interleaved operation ensures a current ripple, which can be considered as sufficiently low for the fuel cell filtering requirements (Section 2.2).

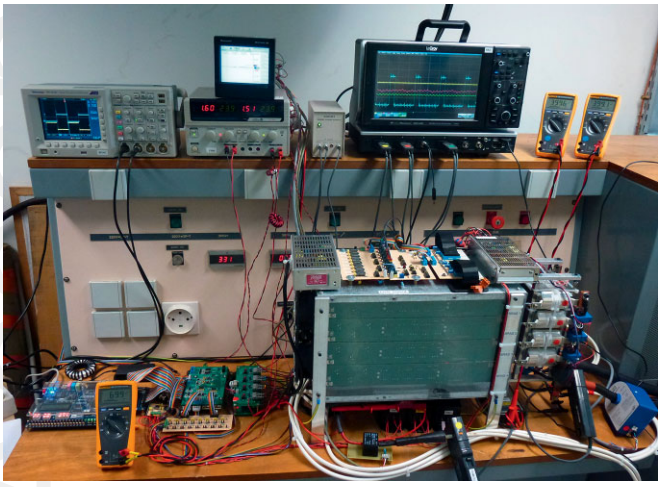

Fig. 10 Experimental setup.

Theoretical and experimental efficiencies of the double boost and proposed converters are shown in Figure 13 [1]. Semi-conductor theoretical losses are deduced from datasheet parameters. ICT losses are estimated using the following Eq. (4):

$$P_{ICT} = k_1 V_{Cell}^2 + k_2 I_{phase}^2 \tag{4}$$

with k_1 = 0.424 mW V^{-2} and k_2 = 47.2 mW A^{-2}. The ICT parameters are determined from a design tool developed at LAPLACE laboratory. The fan cooling system consumes a power equal to 76 W. The experimental efficiencies are obtained using the opposition method to guaranty accurate measures [17]. Experimental curves are shown until phase currents reach 80 A.

As shown in Figure 13, the proposed converter has a higher maximum efficiency (+2%), a flatter efficiency curve and reaches a higher power than the double boost converter (+69%). In terms of loss, the proposed converter has twice less

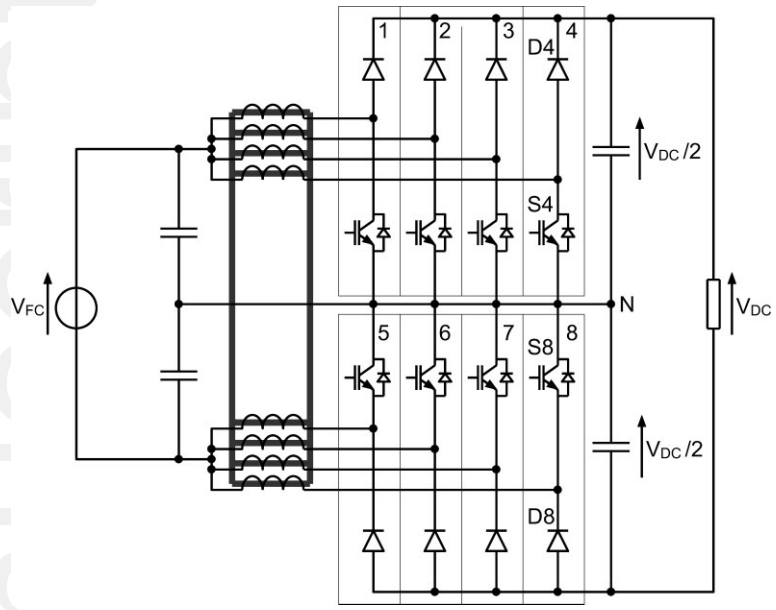

Fig. 11 Electrical schematic of the double boost converter.

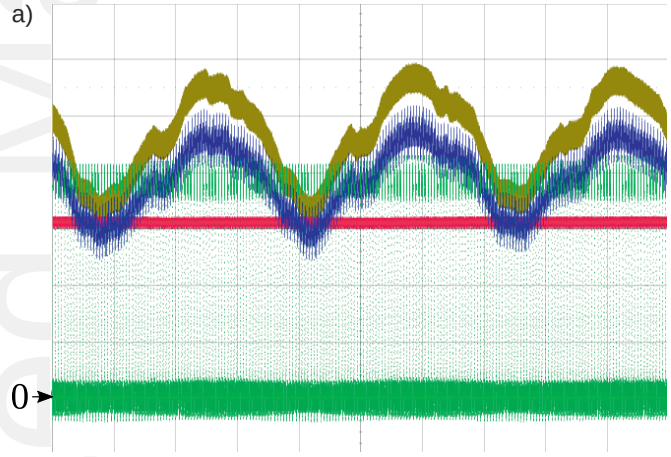

Fig. 12 Fuel cell current I_{FC}, phase current I_2, load current I_{DC}, voltage V_{ph1} (P_{out} = 11.2 kW), with a) 1 ms div^{-1} and b) 1 mm div^{-1}.

loss than the conventional converter at same fuel cell power (Figure 14). More details on this comparison will be given in next sub-section.

4.3 Comparison Between the Proposed Converter and the Double Boost Converter

Figures 15 and 16 show the theoretical losses in the power devices and in the ICT. They illustrate that this proposed mirror topology makes possible to reduce both semiconductor and ICT losses for a same fuel cell power compared to the double boost converter.

This loss reduction is mainly due to the reduction of the phase current for a same fuel cell power as it is shown in Figure 17. And the phase current in the mirror topology is lower than in the double boost thanks to the lower duty cycle of the operation point as shown in Figure 18 (Section 3).

5 Conclusion

An eight-phase interleaved coupled-inductor DC–DC converter has been proposed in this paper. At high voltage conversion ratio it has both the features of series and parallel topologies and has a better ratio of active/freewheeling times which, compared with conventional structures, reduces the penalty induced by the high conversion ratio. Thus, it makes it perfectly suitable for the conversion of low DC voltage source to high DC voltage. The substitution of separate inductors with a monolithic inter-cell transformer (ICT) coupling all converter phases and the interleaved operation make possible the use of smaller passive components. In addition, the inter-

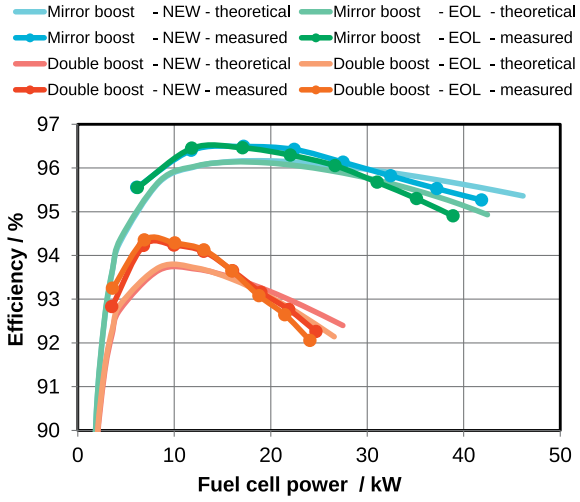

Fig. 13 Theoretical and measured efficiencies of mirror and double-boost converters.

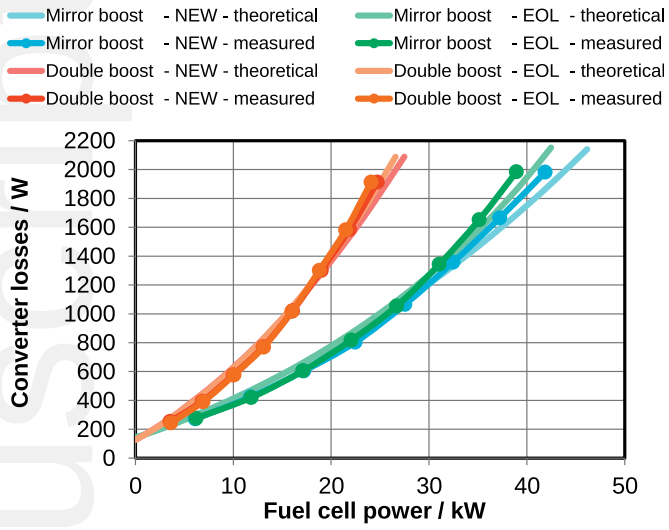

Fig. 14 Theoretical and measured losses of mirror and double-boost converters.

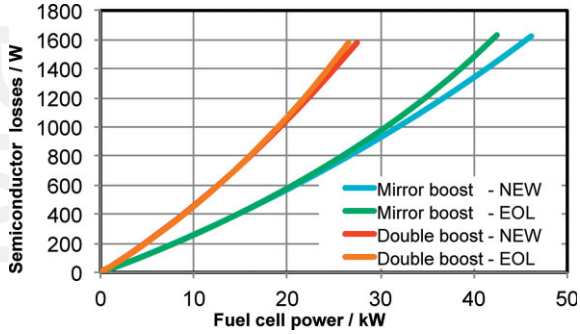

Fig. 15 Semiconductors losses.

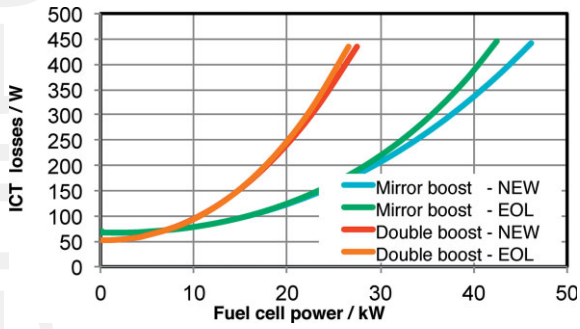

Fig. 16 ICT losses.

leaved technic and the parallel aspect of the proposed converter lead to a source current ripple compatible with fuel cell operation. The proposed converter reaches a peak efficiency of 96.5% at 17 kW and 95.3% at 42 kW for a voltage conversion ratio around 10. Using the same material, experimental results show that the proposed converter achieve twice less loss and a much better specific power than the classical double boost converter. Indeed, it results in a gain of the maximum efficiency of around +2% and a power gain of +69%.

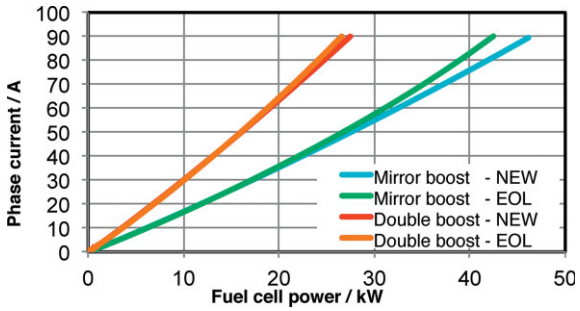

Fig. 17 Current phases.

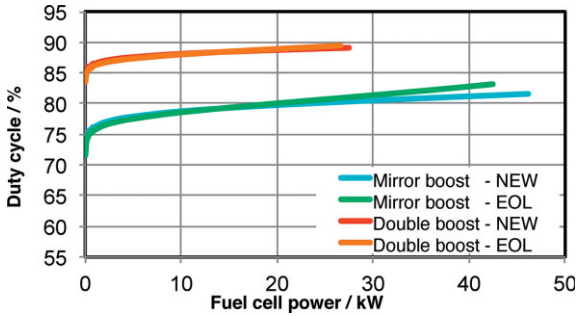

Fig. 18 Duty cycle.

Acknowledgment

The authors would like to thank A. Lacarnoy of Schneider Electric – APC for providing a modular power converter that has been reconfigured for this study.

List of Symbols

CAES	Compressed air energy storage
D	Duty cycle
Elyz	Electrolyzer
EOL	End of life
FC	Fuel cell
ICT	Inter-cell transformer
LF	Low frequency
NEW	Beginning of life
PEC	Power electronics converter
PEM	Proton exchange membrane
PSH	Pumped-stored hydroelectricity

References

[1] N. Videau, *PhD Thesis*, Institut National Polytechnique de Toulouse (INPT), Toulouse, France, **2014**.

[2] M. C. Pera, D. Hissel, H. Gualous, C. Turpin, *Electrochemical Components*, Wiley-ISTE, **2013**.

[3] B. Cougo, *PhD Thesis*, Institut National Polytechnique de Toulouse (INPT), Toulouse, France, **2010**.

[4] M. Calais, J. Myrzik, T. Spooner, V.G. Agelidis, *Proc. of the Power Electronics Specialists Conference 2002*, IEEE 33rd Annual, Cairns, Qld., Australia, **2002**, 4, 1995–2000.

[5] D. Coutelier, V.G. Agelidis, C. Sewan, *Proc of. Power Electronics Specialists Conference, 2008*, IEEE, Rhodes, Greece, **2008**, 562–568.

[6] O. Rallières, *Master Thesis*, Conservatoire National des Arts et Métiers (CNAM), Toulouse, France, **2005**.

[7] F. Forest, T. Meynard, J. J. Huselstein, D. Flumian, C. Rizet, A. Lacarnoy, *IEEE Transactions on Power Electronics* **2014**, *29*, 45.

[8] B. V. Dang, Y. Lembeye, J. P. Ferrieux, J. Barbaroux, Y. Avenas, *Proc. of Power Electronics Specialists Conference 2006,* IEEE 37th, **2006**, 1–7.

[9] K. Kajangpan, B. Neammanee, *Proc. of Electrical Engineering/Electronics, Computer, Telecommunications and Information Technology, 2009*, 6th International Conference on, **2009**, 1, 292–295.

[10] P. Thounthong, P. Sethakul, B. Davat, *IEEE International Conference on Industrial Technology, ICIT 2009*, **2009**, 1.

[11] M. Kabalo, D. Paire, B. Blunier, D. Bouquain, M. Godoy Simões, A. Miraoui, *Power Electronics* **2013**, *6*, 215.

[12] N. Videau, T. Meynard, G. Fontes, D. Flumian, *PCIM Europe 2013,* **2013**.

[13] G. Fontes, C. Turpin, S. Astier, T. Meynard, *IEEE Transactions on Power Electronics* **2007**, *22*, 670.

[14] F. A. De Bruijn, V. A. T. Dam, G. J. M. Janssen, *Fuel Cells* **2008**, *8*, 3.

[15] F. Harel, X. François, D. Candusso, M.-C. Péra, D. Hissel, J.-M. Kauffmann, *Fuel Cells* **2007**, *7*, 142.

[16] D. Guilbert, A. Gaillard, A. Mohammadi, A. N'Diaye, A. Djerdir, *International Journal of Hydrogen Energy* **2015**, *40*, 519.

[17] F. Forest, J. J. Huselstein, S. Faucher, M. Elghazouani, P. Ladoux, T. Meynard, F. Richardeau, C. Turpin, *IEEE Transactions on Industrial Electronics* **2006**, *53*, 530.